LETTER

doi:10.1038/nature13472

Abrupt pre–Bølling–Allerød warming and circulation changes in the deep ocean

Nivedita Thiagarajan[1], Adam V. Subhas[1], John R. Southon[2], John M. Eiler[1] & Jess F. Adkins[1]

Several large and rapid changes in atmospheric temperature and the partial pressure of carbon dioxide in the atmosphere[1]—probably linked to changes in deep ocean circulation[2]—occurred during the last deglaciation. The abrupt temperature rise in the Northern Hemisphere and the restart of the Atlantic meridional overturning circulation at the start of the Bølling–Allerød interstadial, 14,700 years ago, are among the most dramatic deglacial events[3], but their underlying physical causes are not known. Here we show that the release of heat from warm waters in the deep North Atlantic Ocean probably triggered the Bølling–Allerød warming and reinvigoration of the Atlantic meridional overturning circulation. Our results are based on coupled radiocarbon and uranium-series dates, along with clumped isotope temperature estimates, from water column profiles of fossil deep-sea corals in a limited area of the western North Atlantic. We find that during Heinrich stadial 1 (the cool period immediately before the Bølling–Allerød interstadial), the deep ocean was about three degrees Celsius warmer than shallower waters above. This reversal of the ocean's usual thermal stratification pre-dates the Bølling–Allerød warming and must have been associated with increased salinity at depth to preserve the static stability of the water column. The depleted radiocarbon content of the warm and salty water mass implies a long-term disconnect from rapid surface exchanges, and, although uncertainties remain, is most consistent with a Southern Ocean source. The Heinrich stadial 1 ocean profile is distinct from the modern water column, that for the Last Glacial Maximum and that for the Younger Dryas, suggesting that the patterns we observe are a unique feature of the deglacial climate system. Our observations indicate that the deep ocean influenced dramatic Northern Hemisphere warming by storing heat at depth that preconditioned the system for a subsequent abrupt overturning event during the Bølling–Allerød interstadial.

Understanding the cause of abrupt terminations of glacial periods is a central question in palaeoclimate as these rapid warmings characterize the 'sawtooth' nature of glacial cycles[4]. The last deglaciation started ~18 kyr ago in the Southern Hemisphere with an increase in temperature[1] and greenhouse gas concentration[1] and a retreat of sea ice[5]. For over 3 kyr Antarctica warmed while Greenland and the North Atlantic remained cold. This period, known as Heinrich stadial 1 (HS1), ended abruptly 14.7 kyr ago at the start of the Bølling–Allerød, when sea ice retreated in the north[5], the Atlantic meridional overturning circulation (AMOC) restarted[2] and the Northern hemisphere dramatically warmed[1], with a corresponding return to cold conditions in the south[1]. Explanations for the Bølling–Allerød shift have focused on the AMOC restart and include a variety of triggers[6–9]. Here we use coupled U-series and ^{14}C ages and clumped isotope (Δ_{47}; Methods) temperature measurements on deep-sea corals from the New England seamounts to reconstruct ocean temperatures and circulation along a depth transect (Methods). We find that the deep ocean at our site was characterized by warmer waters underneath colder waters ~800 yr before the beginning of the Bølling–Allerød. This unusual scenario implies that salt stratification of the water column stored potential energy at depth, giving the deep ocean a fundamental role in the restart of the AMOC at the beginning of the Bølling–Allerød.

Figure 1 shows new and previously published[10,11] $\Delta^{14}C$ values for the Younger Dryas and two time slices during HS1. Prior to 15.6 kyr ago, the $\Delta^{14}C$ of the water column was offset from the contemporaneous atmosphere by 110–195‰. This value is much larger than the modern North Atlantic offset of ~70‰, implying that the HS1 ocean was less well ventilated (older) than the modern ocean. At that time, $\Delta^{14}C$ decreased from top to bottom in the profile. At 15.6 kyr ago there was a sudden, large shift to even more ^{14}C-depleted waters at intermediate depths. This 'mid-15-kyr' event is observed within the skeletons of two separate corals, JFA 24.8 and JFA 24.19, both found at 1,784 m. As previously reported, this large shift, contemporaneous with a constant $\Delta^{14}C$ at greater depths (2,000–2,400 m), is consistent with a lateral influx of very ^{14}C-depleted, southern-sourced intermediate waters[10,11], implying a water mass boundary at depth between rapidly changing upper waters and less variant deep waters.

The timing of this change in $\Delta^{14}C$ is surprising because these mid-15-kyr changes do not appear to correlate in time with either the air temperature records from Greenland ice cores or the largest changes in atmospheric gas concentration[1]. However, mid-HS1 variability has previously been observed and was first described in the character and source region of icebergs reaching the Iberian margin[12] (called the HS1a–HS1b transition), and pre- Bølling–Allerød changes have been seen in other marine records (Methods). Here we propose a scenario where the mid-15-kyr changes are unique to the intermediate and upper portions of the deep ocean.

The most striking new feature of the deglacial water column comes from a subset of the corals in Fig. 1a–c that we analysed for Δ_{47}-based temperatures (Figs 1d–f and 2). These corals reveal a large (5 °C) and abrupt warming during HS1 in the North Atlantic that is almost contemporaneous with the shift to even more ^{14}C-depleted waters. These signals must arise from the movement of a front across our corals during their lifetime. By running numerous replicates, we were able to shrink the uncertainty in our temperature estimates and confirm that the deep warming is outside the limit of our analytical errors[13] (Methods). This abrupt warming has an important depth structure, as documented by temperature profiles before and after the $\Delta^{14}C$ event (Fig. 1d–f). The pre-15.6-kyr profile is cooler than the modern one and is roughly isothermal, but the younger HS1 profile is cool at 1,381 m and warmer at greater depths. To maintain static stability, this temperature inversion requires that the water column also becomes saltier with depth, a feature that has been previously observed for the Last Glacial Maximum[14] (LGM). If we assume constant potential density (a minimum definition of static stability) between 1,381 and 2,600 m, we calculate that the smallest salt difference needed to support the observed warm deep waters below shallower cooler waters is ~0.8 p.s.u., which is well within the bounds of the LGM ocean[14].

The deglacial coevolution of temperature and $\Delta^{14}C$ at intermediate depths shows three vectors of ocean temperature and $\Delta^{14}C$ behaviour that occur over the course of HS1, one from 17 to 15.8 kyr ago, when the ocean became more depleted in $\Delta^{14}C$ (even relative to the modern atmosphere); one around 15.8 to 15.6 kyr ago, when waters deeper than

[1]Division of Geological and Planetary Sciences, California Institute of Technology, Pasadena, California 91125, USA. [2]Earth System Science Department, 3200 Croul Hall, University of California, Irvine, California 92697–3100, USA.

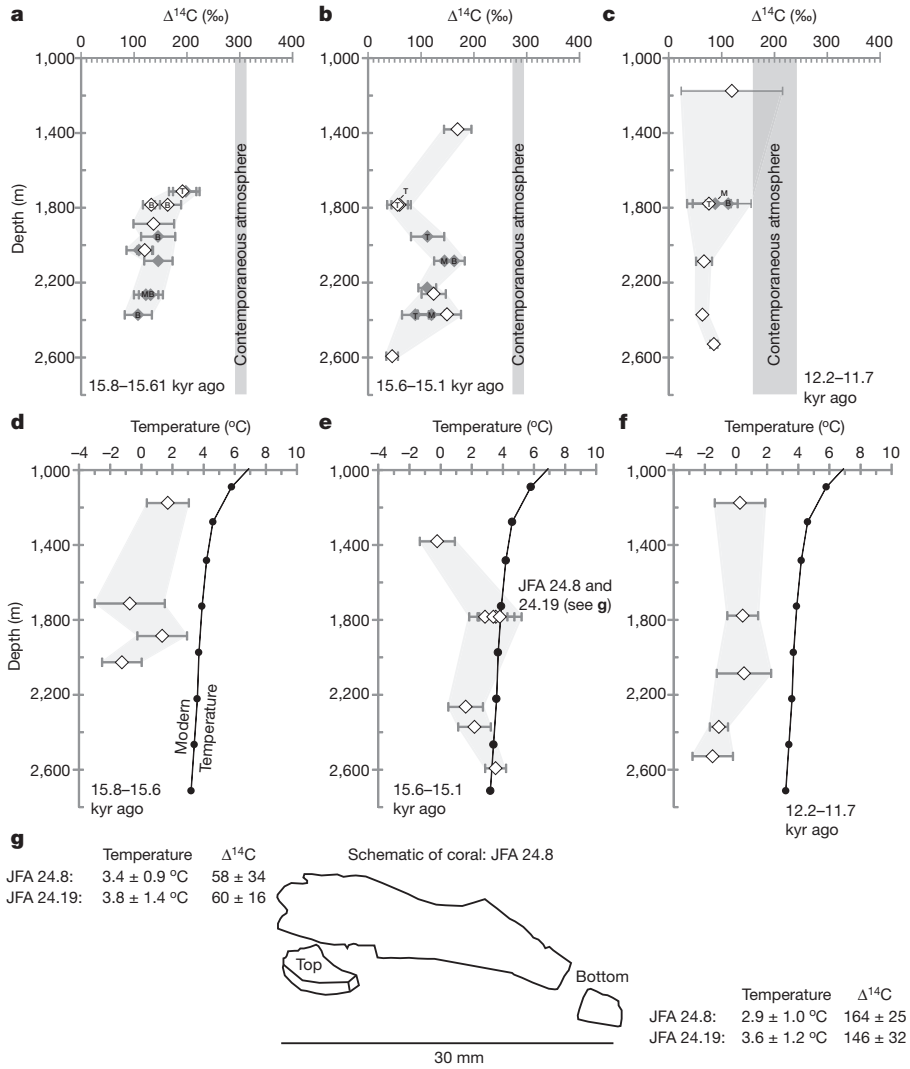

Figure 1 | Ocean profiles of $\Delta^{14}C$ and temperature during three different time intervals. **a**–**c**, $\Delta^{14}C$ profiles. Points outlined in black have also been measured for temperature. There is an abrupt shift in $\Delta^{14}C$ ($\Delta^{14}C = 1{,}000 \times (e^{-{}^{14}C_{age}/8{,}033}/e^{-Cal_{age}/8{,}266} - 1)$, where $^{14}C_{age}$ and Cal_{age} are respectively the radiocarbon age and the calendar age of the coral) at mid-15-kyr. T, M and B refer to analyses made on the top, middle and bottom of a coral sample, respectively. Symbols with no letters refer to the top of the coral. Error bars are 1 s.e.m. **d**–**f**, Temperature profiles. Unlike the $\Delta^{14}C$ profiles, the bottoms of JFA 24.8 and JFA 24.19 are on the 15.6–15.1-kyr panel (**e**). The value of *n* for each measurement is given in Source Data. **g**, Sketch of coral transects. $\Delta^{14}C$ shows an abrupt shift between the tops and bottoms of the two corals, but there is little change in temperature.

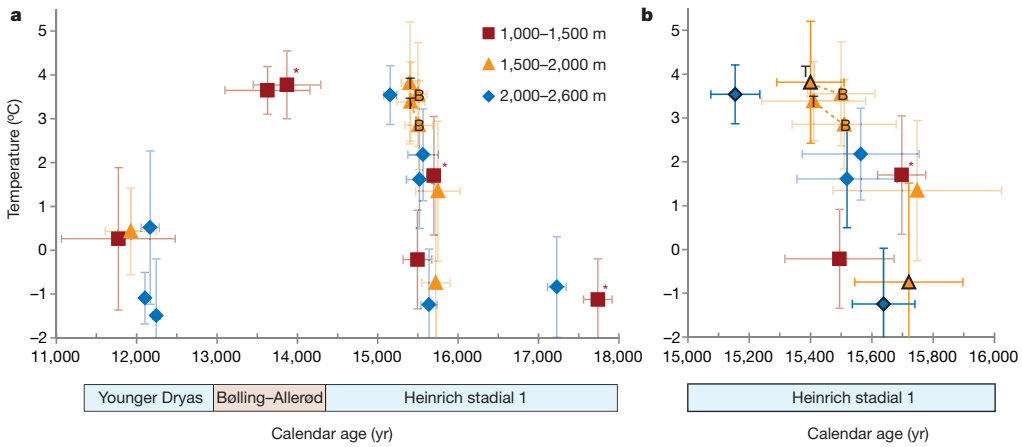

Figure 2 | Temperature versus calendar age based on clumped isotopes in deep-sea corals across the deglaciation. **a**, The dashed lines connect the tops and bottoms of JFA 24.8 and JFA 24.19. T and B refer to the top and bottom of a coral, respectively. Error bars are 1 s.e.m. Asterisks indicate corals that have either a high $\delta^{234}U_i$ (which is the initial $^{234}U/^{238}U$ isotope ratio at the time of coral growth) or a $\Delta^{14}C$ greater than the atmosphere value. In both cases, this open-system behaviour changes the $\Delta^{14}C$ values but does not change calendar ages much on this plot. The value of *n* for each measurement is given in Source Data. **b**, The abrupt warming is encapsulated by the two oldest and youngest corals within this time frame, and these corals are outlined in black.

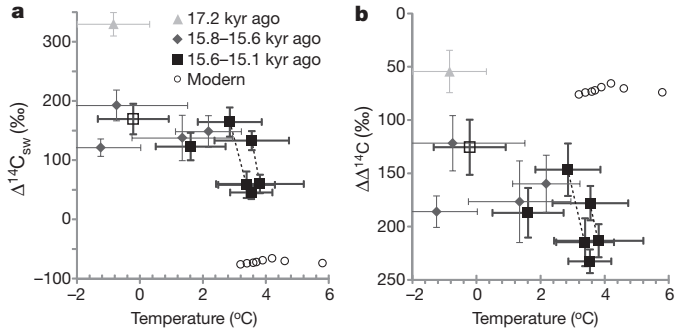

Figure 3 | $\Delta^{14}C$–temperature cross-plot. **a**, Plot of $\Delta^{14}C$ versus temperature for the intermediate-depth waters of the deglacial North Atlantic. The open square is the shallowest HS1 coral, from 1,381 m, and does not warm. The dashed lines connect the tops and bottoms of JFA 24.8 and JFA 24.19. Modern $\Delta^{14}C$ and temperature measurements for our site are from the GEOSECS database. The value of *n* for each measurement is given in Source Data. **b**, Offset of reconstructed deep-sea coral $\Delta^{14}C$ from contemporaneous atmosphere as determined by the Hulu record[30] versus temperature for intermediate depths. Error bars are 1 s.e.m.

1,600 m warmed; and one from 15.6 to 15.1 kyr ago, when those same deeper waters became even more depleted in $\Delta^{14}C$ (Fig. 3). The temperature and $\Delta^{14}C$ transitions are not simultaneous (Fig. 1g); both the tops and the bottoms of corals JFA 24.8 and JFA 24.19 are already warm, and the $\Delta^{14}C$ switch occurs during their lifetime. This offset, although unusual, has several possible explanations. During the deglaciation, the ocean–atmosphere system was not at steady state, and it is therefore possible that multiple reservoirs with different heat and radiocarbon contents influenced our site during HS1. Even for a single water mass, temperature and carbon isotopes have different timescales for exchange at their outcrop region, so they may have been decoupled from each other for ~100 yr during deglaciation. Regardless of the cause of the offset, the warm, $\Delta^{14}C$-depleted water that existed by 15.4 ± 0.2 kyr ago, below a colder upper layer, is a uniquely deglacial feature, with no equivalent in either the modern or the LGM oceans.

The observation of warming at intermediate depths in the Atlantic during HS1 has been controversial. Several regional benthic foraminifera records show depleted $\delta^{18}O$ values that were initially interpreted as a signature of brine rejection in the Nordic Seas[15], but other temperature records attribute the same signal to intermediate or deep ocean warming[16,17]. On the basis of our clumped isotope data, at least ~1‰ of the benthic $\delta^{18}O$ depletion seen in these records is due to warming. Several modelling studies[7,16,18] also show intermediate or deep North Atlantic warming during deglaciation, due to diffusion of tropical ocean heat across the main thermocline during times of slow North Atlantic overturning. If the downward diffusion of heat were local, this scenario would predict monotonically decreasing temperature profiles with depth[16], but we see cold shallow waters above warm deeper waters at the mid-15kyr event. Given the abrupt nature of the warming in our corals, the signal is most probably that of heat that is accumulated elsewhere and quickly brought to ~2,000 m water depth by movement of a deep front.

Other possible sources of heat to the intermediate or deep ocean include geothermal heating[19] and warming of the outcrop region for isopycnals that occupied our site: either could lead to the temperature inversion we observe. Several water masses have been found during Heinrich events to have either warmed or exhibited depleted $\Delta^{14}C$ values, and, although none of these show both signatures simultaneously (Methods), an influx of southern-sourced water to our site could explain our results (Extended Data Figs 6 and 7), because inefficient carbon isotope exchange in the outcrop regions tends to produce low initial $\Delta^{14}C$ values. Heating at the deep-water formation zones in the Southern Hemisphere could be transferred to near our site by the deep circulation. Then a pre-Bølling–Allerød shift in deep-water structure (potentially caused by winds or buoyancy fluxes in the Southern Ocean, or both) could cause this warm front to cross our site from deeper waters to shallower.

Although the geographic origin of the warm deep waters is an important issue, the most significant feature of our new results is that the presence of warm waters below colder waters, supported by salt stratification, is a natural way to build capacitance in the climate system. Warming of the deep ocean can explain the polar records of deglaciation and helps us understand how the ocean moved between the stable glacial and interglacial states of deep circulation.

A new compilation of Atlantic benthic $\delta^{13}C$ over the deglaciation suggests that the transition from HS1 to the Bølling–Allerød is the moment where the ocean switched between these two stable circulation states (Fig. 4 and Extended Data Fig. 8). Sections of $\delta^{13}C$ show a vertically stratified ocean at the LGM with large $\delta^{13}C$ differences between southern and northern endmembers. In the early deglaciation, the upper waters changed more than the deepest waters (Extended Data Fig. 8), reflecting a more dynamic interplay between northern- and southern-sourced intermediate and upper deep waters. This situation changed drastically at the HS1/Bølling–Allerød transition, when the deep southern-sourced[20] water mass became much less depleted and volumetrically less important. Pa/Th records[2,21,22] exhibit similar behaviour during the early deglaciation, with intermediate depth water masses showing a more vigorous circulation than the more stable deep-ocean records[2,22]. This was followed by the HS1/Bølling–Allerød transition, when, according to deep-ocean Pa/Th, the AMOC was reinvigorated. This reinvigoration continued to its modern strength with a small decline during the Younger Dryas.

We suggest that the transition between LGM and modern circulation patterns was facilitated by instabilities in the deep water column. A water column with cold, fresh water on top of warm, salty water, as observed after the mid-15-kyr event, can be susceptible to a finite-amplitude instability, where water parcels rapidly exchange positions vertically to release potential energy stored in as heat in the deep ocean[23]. This condition is analogous to convectively available potential energy in the atmosphere[23]. In the ocean it is thermobaricity[24] that leads to the instability, and its effects are seen in deep-water formation regions today[25] as well as in

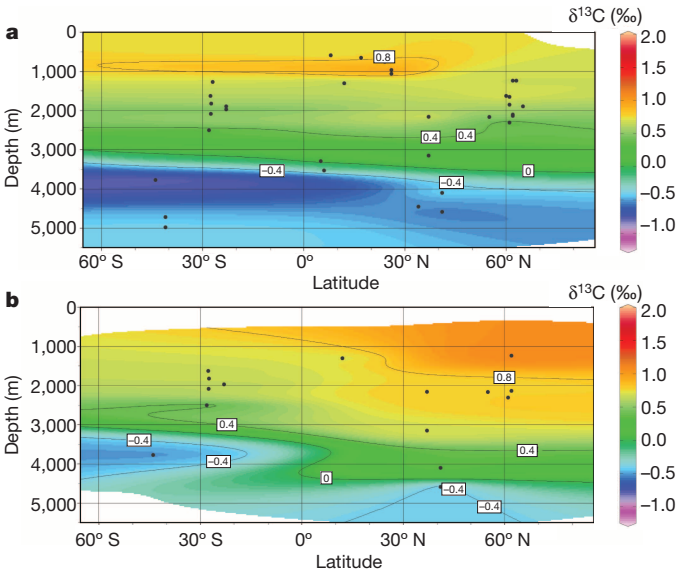

Figure 4 | Benthic sections of $\delta^{13}C$ during late HS1 and the Bølling–Allerød. Well-dated, high-resolution cores from the Atlantic Ocean were chosen from the end of HS1 (14.5–15.7 kyr ago) (**a**) and during the Bølling–Allerød (13–14.5 kyr ago) (**b**). Black dots indicate the latitudes and depths of cores used to make the sections. These time slices come from a larger set across the whole termination (Extended Data Fig. 8), and we display them because they show the largest switch from southern-source-dominated waters in the abyssal Atlantic at the LGM to a more 'interleaved' pattern in the modern. The Bølling–Allerød marks this abrupt shift in deep tracer distribution.

large eddy simulation models of ocean convection[26]. In this scenario, the 'trigger' for the Bølling–Allerød AMOC restart and abrupt warming was not the removal of fresh water from the surface of the North Atlantic[27], but was instead the release of deep-ocean warmth that built up over time. A trigger for the release can always be found by the climate system (breaking internal waves that initiate vertical water movement, and small changes in the buoyancy budget of the surface ocean are two examples) but it is less fundamental to the physics than the build-up of the potential energy itself. Rather than being merely a response to fresh water forcing at the surface[28], the deep ocean circulation has an important role in the forcing of the dramatic Northern Hemisphere warming at the start of the Bølling–Allerød and in the bipolar nature of deglaciations generally. On this view, the Bølling–Allerød represents a fundamental change in the density structure of the deep ocean, when the thermobaric instability of the whole deep water column allowed the system to 'punch through' the LGM stratification and move towards the modern deep Atlantic structure of warm, salty North Atlantic deep water and cold, fresh Antarctic bottom water (Fig. 4). Whereas the Younger Dryas water column in the North Atlantic is often thought of as a return to Heinrich-like water masses, we show that it is structured very differently than the HS1 water column in temperature, $\delta^{13}C$ and $\Delta^{14}C$. Mid-depth warming in the North Atlantic has also been observed at many Heinrich events[16], but only HS1 led to a deglaciation. Future work will have to establish whether salt stratification accompanied these previous temperature changes.

METHODS SUMMARY

Samples examined in this study were obtained from the California Institute of Technology deep-sea coral fossil collection. The deep-sea coral species *Desmophyllum dianthus* from the New England (34–40° N, 60–68° W) and Corner Rise seamounts (34–36° N, 47–53° W) (Extended Data Fig. 1) were collected in 2003–2005 using the deep submergence vehicles *Alvin* and *Hercules*. Collection by remotely operated underwater vehicle and submarine ensured that the depth of each coral was precisely known and that corals were collected near growth positions. All samples in this study were cleaned and analysed for U/Th ages, ^{14}C ages and Δ_{47} temperatures (Supplementary Information).

All samples analysed for ^{14}C and U/Th were physically cleaned and chemically cleaned following previously established procedures[11,29] (Methods). Radiocarbon ages were measured at the UC-Irvine Keck-CCAMS facility on an accelerator mass spectrometer. Uranium-series ages were run on a multi-collector inductively coupled plasma mass spectrometer at Caltech. All samples were bracketed by an instrumental standard of known isotopic composition to correct for mass bias and mass drift.

Clumped isotope measurements were made on the deep-sea corals at the California Institute of Technology following previously established procedures[13]. Deep-sea corals, unlike modern corals, have a Fe–Mn crust, and a cleaning study determined that physical cleaning alone gave accurate clumped isotope temperatures (Extended Data Fig. 2). Samples were analysed multiple times ($n = 3$–20) to ensure low external standard errors.

Benthic $\delta^{13}C$ sections were made by compiling well-dated, high-resolution benthic $\delta^{13}C$ records (Methods).

Online Content Methods, along with any additional Extended Data display items and Source Data, are available in the online version of the paper; references unique to these sections appear only in the online paper.

Received 19 August 2013; accepted 7 May 2014.

1. Petit, J.-R. *et al.* Climate and atmospheric history of the past 420,000 years from the Vostok ice core, Antarctica. *Nature* **399,** 429–436 (1999).
2. McManus, J., Francois, R., Gherardi, J., Keigwin, L. & Brown-Leger, S. Collapse and rapid resumption of Atlantic meridional circulation linked to deglacial climate changes. *Nature* **428,** 834–837 (2004).
3. Clark, P. U. *et al.* Global climate evolution during the last deglaciation. *Proc. Natl Acad. Sci. USA* **109,** E1134–E1142 (2012).
4. Broecker, W. S. & van Donk, J. Insolation changes, ice volumes, and the O18 record in deep-sea cores. *Rev. Geophys.* **8,** 169–198 (1970).
5. Denton, G. H., Alley, R. B., Comer, G. C. & Broecker, W. S. The role of seasonality in abrupt climate change. *Quat. Sci. Rev.* **24,** 1159–1182 (2005).
6. Weaver, A. J., Saenko, O. A., Clark, P. U. & Mitrovica, J. X. Meltwater pulse 1A from Antarctica as a trigger of the Bølling-Allerød warm interval. *Science* **299,** 1709–1713 (2003).
7. Liu, Z. *et al.* Transient simulation of last deglaciation with a new mechanism for Bølling-Allerød warming. *Science* **325,** 310–314 (2009).
8. Rogerson, M. *et al.* Enhanced Mediterranean-Atlantic exchange during Atlantic freshening phases. *Geochem. Geophys. Geosyst.* **11,** Q08013 (2010).
9. Knorr, G. & Lohmann, G. Southern Ocean origin for the resumption of Atlantic thermohaline circulation during deglaciation. *Nature* **424,** 532–536 (2003).
10. Adkins, J. F., Cheng, H., Boyle, E. A., Druffel, E. R. M. & Edwards, L. Deep-sea coral evidence for rapid change in ventilation of the deep North Atlantic 15,400 years ago. *Science* **280,** 725–728 (1998).
11. Robinson, L. F. *et al.* Radiocarbon variability in the western North Atlantic during the last deglaciation. *Science* **310,** 1469–1473 (2005).
12. Bard, E., Rostek, F., Turon, J.-L. & Gendreau, S. Hydrological impact of Heinrich events in the subtropical Northeast Atlantic. *Science* **289,** 1321–1324 (2000).
13. Thiagarajan, N., Adkins, J. & Eiler, J. Carbonate clumped isotope thermometry of deep-sea corals and implications for vital effects. *Geochim. Cosmochim. Acta* **75,** 4416–4425 (2011).
14. Adkins, J. F., McIntyre, K. & Schrag, D. P. The salinity, temperature, and d18O of the glacial deep ocean. *Science* **298,** 1769–1773 (2002).
15. Dokken, T. & Jansen, E. Rapid changes in the mechanism of ocean convection during the last glacial period. *Nature* **401,** 458–461 (1999).
16. Marcott, S. A. *et al.* Ice-shelf collapse from subsurface warming as a trigger for Heinrich events. *Proc. Natl Acad. Sci.* **108,** 13415–13419 (2011).
17. Rasmussen, T. L., Thomsen, E., Labeyrie, L. & van Weering, T. C. E. Circulation changes in the Faeroe-Shetland Channel correlating with cold events during the last glacial period (58–10 ka). *Geology* **24,** 937–940 (1996).
18. Shaffer, G., Olsen, S. M. & Bjerrum, C. J. Ocean subsurface warming as a mechanism for coupling Dansgaard-Oeschger climate cycles and ice-rafting events. *Geophys. Res. Lett.* **31,** L24202 (2004).
19. Stein, C. A. & Stein, S. A model for the global variation in oceanic depth and heat-flow with lithospheric age. *Nature* **359,** 123–129 (1992).
20. Kwon, E. Y. *et al.* North Atlantic ventilation of "southern-sourced" deep water in the glacial ocean. *Paleoceanography* **27,** PA2208 (2012).
21. Gherardi, J.-M. *et al.* Evidence from the Northeastern Atlantic basin for variability in the rate of the meridional overturning circulation through the last deglaciation. *Earth Planet. Sci. Lett.* **240,** 710–723 (2005).
22. Gherardi, J. *et al.* Glacial–interglacial circulation changes inferred from $^{231}Pa/^{230}Th$ sedimentary record in the North Atlantic region. *Paleoceanography* **24,** PA2204 (2009).
23. Adkins, J. F., Ingersoll, A. P. & Pasquero, C. Rapid climate change and conditional instability of the glacial deep ocean from the thermobaric effect and geothermal heating. *Quat. Sci. Rev.* **24,** 581–594 (2005).
24. McDougall, T. Thermobaricity, cabbeling, and water-mass conversion. *J. Geophys. Res.* **92,** 5448–5464 (1987).
25. Denbo, D. W. & Skyllingstad, E. D. An ocean large-eddy simulation model with application to deep convection in the Greenland Sea. *J. Geophys. Res.* **101,** 1095–1110 (1996).
26. Akitomo, K. Open-ocean deep convection due to thermobaricity 1. Scaling argument. *J. Geophys. Res.* **104,** 5225–5234 (1999).
27. Ganopolski, A. & Rahmstorf, S. Rapid changes of glacial climate simulated in a coupled climate model. *Nature* **409,** 153–158 (2001).
28. Rahmstorf, S. Bifurcations of the Atlantic thermohaline circulation in response to changes in the hydrological cycle. *Nature* **378,** 145–149 (1995).
29. Adkins, J. F. *et al.* Radiocarbon dating of deep-sea corals. *Radiocarbon* **44,** 567–580 (2002).
30. Southon, J., Noronha, A. L., Cheng, H., Edwards, R. L. & Wang, Y. A high-resolution record of atmospheric ^{14}C based on Hulu Cave speleothem H82. *Quat. Sci. Rev.* **33,** 32–41 (2012).

Supplementary Information is available in the online version of the paper.

Acknowledgements We thank J. McManus and M. Miller for discussions. We also thank the captain and crew of the RV *Atlantis* cruise AT7-35 and the WHOI Deep Submergence Alvin and ABE groups.

Author Contributions N.T. and J.F.A. designed the study. N.T. collected the ^{14}C and Δ_{47} data and compiled the benthic $\delta^{13}C$ sections. J.R.S. facilitated and oversaw the ^{14}C measurements and J.M.E. facilitated and oversaw the Δ_{47} measurements. A.V.S. collected the U-series data. J.F.A. facilitated and oversaw the U-series measurements. N.T. and J.F.A. wrote the first draft of the manuscript. All authors contributed to the interpretation and preparation of the final manuscript.

Author Information Reprints and permissions information is available at www.nature.com/reprints. The authors declare no competing financial interests. Readers are welcome to comment on the online version of the paper. Correspondence and requests for materials should be addressed to N.T. (nivedita@gps.caltech.edu).

METHODS

Sample collection. Samples examined in this study were obtained from the Caltech deep-sea coral fossil collection. The deep-sea coral species *Desmophyllum dianthus* from the New England (34–40° N, 60–68° W) and Corner Rise seamounts (34–36° N, 47–53° W) (Extended Data Fig. 1) were collected in 2003–2005 using the deep submergence vehicles *Alvin* and *Hercules*. Collection by remotely operated underwater vehicle and submarine ensured that the depth of each coral was precisely known and that corals were collected near growth positions. We selected for the study on the basis of the reconnaissance age screening[31], which yielded sufficient specimens to form depth transects spanning 1,200–2,600 m in the water column during HS1 and the Younger Dryas. Two additional corals, JFA 24.8 and JFA 24.19[10], were analysed for Δ_{47} temperatures along the top and bottom of each sample.

Radiocarbon dating method. All samples analysed for ^{14}C and U/Th were pre-cleaned according to established methods[1]. Briefly, the corals were first physically cleaned with a Dremel tool followed by chemical cleaning: ultrasonicating alternately in $NaOH/H_2O_2$ and MILLI Q water, and then rinsing with methanol and briefly leaching in $HClO_4/H_2O_2$[29]. After pre-cleaning, 1 g of coral was removed for U/Th analysis. Twenty milligrams of coral was then taken to UC-Irvine for radiocarbon analysis. There, immediately before phosphoric acid dissolution and graphitization, each sample was leached in HCl to remove ~50% of its total mass. The resulting coral was hydrolysed in phosphoric acid, and the evolved CO_2 was graphitized under H_2 on an iron catalyst for ^{14}C analysis[29]. Radiocarbon ages were measured at the UC-Irvine-Keck-CCAMS facility on an accelerator mass spectrometer. Radiocarbon results are normalized to a $\delta^{13}C = -25‰$ and are reported as fraction modern (Fm), where 'modern' is defined as 95% of the radiocarbon concentration of NBS Oxalic Acid I (NIST-SRM-4990) normalized to a $\delta^{13}C = -19‰$ and reported as radiocarbon age using the following equation: $^{14}C\ age = -8{,}033\ln(Fm)$.

Uranium-series methods. One gram of pre-cleaned coral was processed to extract U and Th following established methods[32]. Corals were dissolved in concentrated Seastar nitric acid and spiked with a ^{229}Th-^{236}U double spike. Uranium and thorium were scavenged from the resulting solution by iron co-precipitation. The iron pellet was then dissolved in 8 N Seastar nitric acid. Uranium and thorium fractions were separated using trace-metal-clean Teflon columns and a Bio Rad AG-1X-8 cation exchange resin. Eluted fractions were dried down several times after successive dropwise additions of concentrated perchloric acid and Seastar nitric acid.

Uranium fractions were brought up in ~500 µl 5% Seastar nitric acid. Samples (but not chemistry blanks) were then intensity-matched for ^{234}U to within 5–10% of the instrumental standard (CRM-145, opened and diluted in winter 2010). ^{234}U was measured on the centre SEM with a retarding potential quadrupole to minimize abundance sensitivity effects. All samples were bracketed by CRM-145 to correct for mass bias and mass drift. Procedural blanks for ^{238}U and ^{234}U accounted for less than 0.04% of the sample signal (76 pg and 3.6 fg, respectively).

Thorium fractions were run separately, also in 5% Seastar nitric acid. ^{229}Th and ^{230}Th were measured on Channeltron ion counters; ^{232}Th was measured on a Faraday cup. The ^{229}Th and ^{230}Th beams were kept below 35,000 c.p.s. in order to maintain the lifetime and linearity of the ion counters. All Th samples were sample–standard-bracketed with an in-house SGS (cross-calibrated in 2010 with an older SGS and CRM-145). No significant errors were introduced by calibrating the Th SGS with a uranium standard, with either a linear or an exponential mass biasing law. In order to determine the amount of initial ^{230}Th originating from the Th-rich ferromanganese crust, a $^{230}Th/^{232}Th$ ratio of $(80 \pm 80) \times 10^{-6}$ was applied to the measured ^{232}Th concentration[33]. Procedural blanks for ^{230}Th and ^{232}Th measured 4 and 22 pg, respectively. ^{232}Th originating from the ferromanganese crust also contributed significantly to the uncertainty in the age measurement, with an average value of 611 pg for all measured corals.

$\delta^{234}U$ values were determined for the corals to test for closed-system behaviour. The reference frame for $\delta^{234}U$ is secular equilibrium (that is, an activity ratio of 1). If the $\delta^{234}U_i$ of the coral is not within the error of modern seawater $\delta^{234}U$ (147‰) then open-system behaviour is assumed and the coral is not used for the $\Delta^{14}C$ calculation. Seawater $\delta^{234}U$ might have been lower during the last glacial period (142‰), so we checked whether our coral $\delta^{234}U$ values were consistent with a step change in the $\delta^{234}U$ of sea water to lower values before 17 kyr ago, following the recommendations of INTCAL09[34]. All but two corals lie within the $\delta^{234}U$ measurement uncertainty of the error envelope of the two potential $\delta^{234}U$ seawater curves determined by INTCAL09[34]. These corals are not included with $\Delta^{14}C$ plots but are included in temperature plots and are indicated with a star. We chose to keep them out of the $\Delta^{14}C$ calculation because this number is very sensitive to the errors in the U-series and radiocarbon dates, but the age errors for comparison with the temperature history are relatively small.

Δ_{47} analysis. Deep-sea corals were first physically cleaned with a Dremel tool. Fossil corals, unlike modern corals, typically have a Fe–Mn crust surrounding them. This crust contains trapped organic matter, and can skew isotopic measurements of the bulk coral. In order to determine the best method for removing the Fe–Mn crust, a cleaning study was performed on a modern coral and a coral with an Fe–Mn crust from Tasmania that had the same radiocarbon age as the modern ocean water from which it was collected (Extended Data Fig. 2). Corals were cleaned in four different ways. The first was only physical cleaning with a Dremel tool, the second was physical cleaning and chemical cleaning with 1:1 H_2O_2:NaOH, the third was physical cleaning and chemical cleaning with 1:1 H_2O_2:NaOH and MeOH, and the fourth was physical cleaning and chemical cleaning with 1:1 H_2O_2:NaOH, MeOH and 2% $HClO_4$. All the chemical cleaning procedures dissolve part of the coral skeleton as well as the Fe–Mn crust and reorganize the clumped signature. Physical cleaning with a Dremel tool was the only method that yielded expected temperatures.

Corals were analysed for Δ_{47} temperatures using previously established methods[35]. Fossil corals were first cleaned with a Dremel tool and powdered with a mortar and pestle. Samples were dissolved in 105% H_3PO_4 at 90 °C. The evolved CO_2 was separated from H_2O using a dry-ice/ethanol trap. The CO_2 was further purified from other incondensable gases using a Porapak Q 120/80 mesh column held at −20 °C. The resulting CO_2 was again purified using dry-ice/ethanol and nitrogen traps and expanded into the bellows of the mass spectrometer. The evolved CO_2 was analysed in a dual-inlet Finnigan MAT-253 mass spectrometer with the simultaneous collection of ion beams corresponding to cardinal masses 44–49 to obtain Δ_{47}, Δ_{48}, Δ_{49}, $\delta^{13}C$ and $\delta^{18}O$ values[13]. The mass-47 beam is composed of $^{17}O^{13}C^{17}O$, $^{17}O^{12}C^{18}O$ and predominantly $^{18}O^{13}C^{16}O$, and we define R^{47} as the abundance of mass 47 isotopologues divided by the mass-44 isotopologue ($R^{47} = [^{17}O^{13}C^{17}O + {}^{17}O^{12}C^{18}O + {}^{18}O^{13}C^{16}O]/[^{16}O^{12}C^{16}O]$). Δ_{47} is reported relative to a stochastic distribution of isotopologues for the same bulk isotopic composition ($\Delta_{47} = (((R^{47}_{measured}/R^{47}_{stochastic}) - 1) - ((R^{46}_{measured}/R^{46}_{stochastic}) - 1) - ((R^{45}_{measured}/R^{45}_{stochastic}) - 1)) \times 1{,}000$). Mass 48 was monitored to detect any hydrocarbon contamination. Measurements of each gas were analysed at 16 V of mass 44 and consisted of eight acquisitions, each of which involved seven cycles of sample–standard comparison with an ion integration time of 26 s per cycle. Internal standard errors of this for Δ_{47} ranged from 0.004‰ to 0.02‰, while external standard errors ranged from 0.003‰ to 0.011‰ (0.5–2.3 °C). The internal standard error for $\delta^{13}C$ ranged from 0.5 to 80 p.p.m., and the internal standard error for $\delta^{18}O$ ranged from 0.9 to 36 p.p.m. The Δ_{47} raw data was corrected for instrument nonlinearity, scale compression and acid reaction temperature[35,36]. The samples were then normalized to carbonate standards run in each session. Samples were corrected for instrument nonlinearity by normalizing sample Δ_{47} to a 'heated gas line' evaluated at $\Delta_{47SA\text{-}WG}$. This normalization was done using $\Delta_{47,SA\text{-}HG} = \Delta_{47,SA\text{-}WG} - \Delta_{47,HG\text{-}WG}$, where $\Delta_{47HG\text{-}WG} = m\delta_{47SA\text{-}WG} + b$ and m and b are respectively the slope and intercept of a heated gas line. Several heated gases of various bulk isotopic compositions were run during each session. Samples were corrected for 'scale compression' by multiplying $\Delta_{47SA\text{-}HG}$ by a factor proportional to the intercept of the heated gas line: $\Delta_{47SA\text{-}HGuncompressed} = \Delta_{47,SA\text{-}HG}(-0.8453/b)$, where b is the intercept of the heated gas line (−0.8453 is the value of heated gas intercept of the heated gas line during the T–Δ_{47} calibration reported in ref. 37). This scale compression changes over the course of time and is different for different instruments. Samples were also corrected for the different acid digestion bath temperatures. This study was conducted at a phosphoric acid temperature of 90 °C, as opposed to the 25 °C temperature used for the inorganic[37] and deep-sea coral calibration studies[38]. Samples were then corrected in the following way: $\Delta_{47SA\text{-}HG,acid} = \Delta_{47SA\text{-}HG,uncompressed} + 0.081$. The additive term 0.081‰ is based on replicate analyses of carbonate standards at 90 °C, which can be traced to the original calibration[35]. Finally, samples were normalized to carbonate standards with previously determined Δ_{47}, which were run and corrected in the same way as unknown samples. Samples were corrected using the following equation: $\Delta_{47SA\text{-}HG,acidtrue} = m_{STD}\Delta_{47SA\text{-}HG,acidmeas} + b_{STD}$. Here m_{STD} and b_{STD} are determined from the carbonate standards: $\Delta_{47STD\text{-}HG,acidtrue} = m_{STD}\Delta_{47STD\text{-}HG,acidmeas} + b_{STD}$. Several carbonate standards as well as 45923, a modern deep-sea coral from 7° N, 56° W, 1,318 m, whose temperature of growth is 4.7 °C, were used for the standard correction scheme. In three sessions, the modern deep-sea coral standard was not run, and the average of the remaining carbonate standards was used instead of using a regression of all carbonate standards. Neither standard correction scheme changes our interpretations.

Benthic $\delta^{13}C$. Benthic $\delta^{13}C$ sections were made by compiling well-dated, high-resolution benthic $\delta^{13}C$ records[39–43]. The published age models were used to determine ages, and sections were made using ODV.

Pre-Bølling–Allerød changes (mid-HS1 variability) seen in other records. Mid-HS1 variability has previously been seen and was first described in the character and source region of icebergs reaching the Iberian margin[12] (called the HS1a–HS1b transition). Other pre-Bølling–Allerød changes, consistent with the timing of our mid-15-kyr event, are seen in sea surface temperature records from the subpolar North Pacific[44], and benthic temperature records from the deep North Atlantic[45] and Southern Ocean[46]. An Atlantic compilation of $\Delta^{14}C$ records also shows that deep cores in the South Atlantic and corals from the Drake passage all converged to a value of ~50‰ before the Bølling–Allerød, a value very close to what we measure

at the New England seamounts (Extended Data Fig. 6f). U-series dates from stalagmites in China show that the maximum extent of drying occurred at 16.1 ± 0.6 kyr ago[47], several hundred years earlier than the changes seen at our site. The link between mid-HS1 changes seen in terrestrial and marine records is an avenue for further research.

Calculation of $\Delta^{14}C$ and $\Delta\Delta^{14}C$. Coupled U-series and 14C ages give a direct measure of the past $\Delta^{14}C$ (ref. 48), a measurement of the time a water mass has been isolated from the atmosphere. Both the radiocarbon age of the coral and the calendar age of the coral (U/Th age) are needed to reconstruct the $\Delta^{14}C$ of seawater: $\Delta^{14}C_{sw} = 1{,}000 \times (e^{-{}^{14}C_{age}/8{,}033} / e^{-Calage/8{,}266} - 1)$ (ref. 48).

To calculate $\Delta\Delta^{14}C$, $\Delta^{14}C_{sw}$ was subtracted from the contemporaneous atmosphere value: $\Delta\Delta^{14}C = \Delta^{14}C_{atmosphere} - \Delta^{14}C_{sw}$. The Hulu atmospheric $\Delta^{14}C$ record, interpolated to the calendar age of the corals, was used as the reference frame[30]. The atmospheric $\Delta^{14}C$ record was also examined over $\pm 2\sigma$ around the calendar age of the coral to determine the range of $\Delta^{14}C_{atmosphere}$ at this time in the past. The standard error of this range was then propagated through the calculation of $\Delta\Delta^{14}C$ to determine the uncertainty in the final $\Delta^{14}C$ value. For corals where $\Delta^{14}C$ and $\Delta\Delta^{14}C$ was measured along a transect of the coral (JFA 24.8 and JFA 24.19), the corals are assumed to have a growth rate of 1 mm yr^{-1} (ref. 33) with a lifetime of 100 yr. Therefore "Top", "Middle" and "Bottom" are assumed to be ~50 yr offset from each other.

Estimation of Δ_{47} uncertainty. A typical internal standard error in a clumped isotope measurement for 16V of mass-44 CO_2 measured for eight acquisitions with an ion integration time of 26 s per cycle is ~0.01‰, which corresponds to 2 °C (1σ). We wanted much smaller standard errors for our measurements than the ±2 °C corresponding to a single measurement, because deep-sea temperature changes were expected to be small. We have previously determined that for deep-sea corals[38], increasing the number of replicate measurements can drive down the errors to as low as <1 °C. Therefore, we measured each deep-sea coral at least three times. Most coral samples were analysed at least seven times and some as many as 20. These large numbers of replicate measurements of corals run over three years resulted in very small errors, as low as ±0.5 °C. For the entire population of deep-sea corals, the external standard error ranged from 0.5 to 2.3 °C, with an average of 1.2 °C.

For each individual measurement we also propagated the uncertainty in the acid temperature correction (0.0024‰)[35], the uncertainty for the Δ_{47} temperature equation (0.005‰)[37] and errors from the corresponding heated gas line. The Δ_{47} temperature equation error may be an overestimate, as several other calibration studies agree with the original Caltech Δ_{47} temperature equation[37] and have significantly reduced the errors of the equation.

Appropriateness of the inorganic Δ_{47}–temperature calibration for deep-sea corals. Deep-sea corals have previously been calibrated to the clumped isotope thermometer using a suite of modern corals from a variety of depths and ocean basins at temperatures from 2 to 25 °C (ref. 13). In the current study, the coldest calculated temperatures are −1 °C. We think it is appropriate to extrapolate the clumped isotope thermometer to −1 °C because of the short range of extrapolation from the calibration curve. The functional dependence of clumping reactions on temperature is not arbitrary. There have been several different calibration studies of carbonates[49,50] with Δ_{47}–T relationships essentially identical to the inorganic clumped isotope calibration curve. This means that the constraint on the Δ_{47}–T slope is very tight and the permitted extrapolations to −1 °C all give the same result.

Calculation of the rate of warming at the mid-15-kyr event. Our data show a rapid warming of several degrees occurring over a few hundred years (Fig. 2b). We see that there is temporal structure in this data outside the age error bars that clearly shows the rapid warming is not just a cloud of points. This warming is seen between 1,500 and 2,600 m water column depth. Between 1,500 and 2,000 m, the warming is spanned by two corals, JFA 24.8 top and NT 012 (whose error bars do not overlap in temperature and age), that show an increase of 4.7 ± 2.7 °C over 321 ± 208 yr. Between 2,000 and 2,600 m, the warming is spanned by NT 022 and NT 016 (whose error bars do not overlap in temperature and age), which show a similar warming of 4.8 ± 1.5 °C over 484 ± 130 yr. These warming rates must occur as a result of the movement of a front across our corals during their lifetime. We do not mean to imply that these data support heating rates of deep ocean water of this magnitude.

Calculation of timescales for various processes to cause heating at our site. Away from spreading centres with hydrothermal activity, where the heat flux is much higher, there is ~100 mW m^{-2} of heat diffusing out of the Earth's crust[19]. Given the heat capacity of sea water, it will take ~2,500 yr for this heat to warm a 2 km-thick water mass at the bottom of the ocean by 1 °C. This is too slow a heating rate, over too thick a water mass, to be the direct cause of heating we see in the deep-sea corals. However, this calculation assumes the heat is accumulating in a stagnant water mass. In reality the bottom temperature is a balance of diffusive fluxes and the advective flux of heat from the overturning circulation, such that the steady-state temperature of geothermally heated bottom water will scale inversely with the overturning rate. We construct a simple box model of this system in Extended Data Fig. 3. Steady-state results for a range of southern cell overturning rates and vertical diffusivities are shown in Extended Data Fig. 4a. For a well-flushed southern cell (10 Sv of overturning) the bottom water is warmed by about 0.8 °C relative to the restoring temperature in the atmosphere, which is roughly equivalent to observations[51]. For very slow overturning (1 Sv) this temperature increase can reach over 8 °C. We then look at the effect of increasing the Southern Ocean restoring temperature relative to the Northern Hemisphere restoring temperature (to simulate warming in the Southern hemisphere, which is known to have happened in the early deglaciation[1]) (Extended Data Fig. 4b). We find that the temperature increase can be as much as 11 °C for low overturning rates. We finally look at the transient solution (Extended Data Fig. 5), where we keep the vertical diffusivity constant and the Southern Hemisphere restoring temperature at 277 K (four degrees warmer than the northern restoring temperature). We find that there is a rapid warming within the first few thousand years. In each case there is large amount of heat storage in deep waters, which requires salt stratification, and this heat storage could be part of the high temperatures brought to our site during HS1.

Another possible heat source for intermediate or deep waters is solar heat moving across the main thermocline by vertical diffusion. To calculate this heat flux, we use Fick's first law of diffusion ($J = -D\delta C/\delta x$), where J is the diffusion flux, D is the diffusion coefficient (10^{-5} m s^{-2}), δC is the temperature change across the thermocline (~15 °C) and δx is the thickness of the main thermocline (1,000 m). These numbers give a tropical thermocline heat flux to the intermediate-depth ocean of ~0.6 W m^{-2}. While larger than the geothermal heating flux, solar heating would similarly require a large change in deep-water residence time to raise the temperature of a 2 km-thick parcel of water by 5 °C. Additionally, our observed warming is at depth, opposite to the profile predicted for diffusion across the main thermocline, making this unlikely to be the direct cause of the warmth. However, like geothermal heat, diffusion of solar heat at low latitudes could accumulate in slowly overturning water and then be advected to our site during HS1.

Comparison of $\Delta^{14}C$ with other Atlantic $\Delta^{14}C$ records. In the literature there are other Atlantic water masses that have either warmed or have a depleted $\Delta^{14}C$ during the deglaciation. We explore these water masses and find the Southern Ocean is probably the most likely to explain the $\Delta^{14}C$ depletion and warmth seen at our site. In Extended Data Fig. 6a, the deep-sea coral and foraminifera data from the New England seamounts are plotted and the three corals showing a warm and $\Delta^{14}C$-depleted signature at 15 kyr ago are circled in red. The water masses that have been proposed to have either warmed or have a $\Delta^{14}C$-depleted signature are the tropical Atlantic[52], brines from Iceland[53], the Mediterranean (as seen in the Mediterranean records[54,55] and in the Iberian Margin[56,57]) and the Southern Ocean[58–61]. First, it would be difficult for tropical and Mediterranean waters to reach the deeper depths at our site. The $\Delta^{14}C$ of thermocline and deep-dwelling planktonic foraminifera in the tropical Atlantic has been previously measured and determined to be almost constantly offset from the atmosphere by only ~100‰ during HS1[62] (Extended Data Fig. 6b). Therefore, despite the tropical Atlantic being warm, it cannot explain the $\Delta^{14}C$-depleted signature seen at the mid-15-kyr event at our site. The $\Delta^{14}C$ of surface corals[55] and foraminifera[54] in the Mediterranean has been measured and in general the $\Delta^{14}C$ is similar to the atmospheric curve (Extended Data Fig. 6d). The Mediterranean was not as depleted in $\Delta^{14}C$ as our site, as it has a $\Delta^{14}C$ of ~150‰ at 15 kyr ago while the warm and $\Delta^{14}C$-depleted deep-sea corals have a $\Delta^{14}C$ of ~0‰. During Heinrich stadials 3 and 4, a benthic Mg/Ca record from the Iberian margin showed evidence of mid-Heinrich stadial warming[56]. This warming was attributed to an influx of Mediterranean overflow waters to the site in question. Our data does not make any statements about mid-HS3 and mid-HS4 warning; however, during HS1, although there are $\Delta^{14}C$-depleted waters bathing the Iberian margin at 3,200 m (Extended Data Fig. 6e), temperatures remain much cooler and there is no pre-Bølling–Allerød abrupt warming event. Instead the Iberian margin warms only several hundred years later at the start of the Bølling–Allerød (Extended Data Fig. 7). Therefore, although the Iberian margin has previously been used to argue mid-Heinrich stadial warmings caused by an increase in Mediterranean overflow waters, we do not see any evidence for an increase in Mediterranean overflow waters to the Iberian margin or to our site. Finally, the Iceland margin has also been previously examined for $\Delta^{14}C$ during the deglaciation[53]. The $\Delta^{14}C$ seen at two depths are extremely depleted, which has been explained as being a result of brine formation in the Nordic seas (Extended Data Fig. 6c). Indeed at 15 kyr ago, the Icelandic margin had $\Delta^{14}C$ values similar to our $\Delta^{14}C$-depleted deep-sea corals. However it is unlikely that brines travelled to our site to impart this $\Delta^{14}C$-depleted signature, as brine formation will produce cold waters and not the warm waters that we see. Extended Data Fig. 5f shows a compilation of $\Delta^{14}C$ from the Southern ocean (AAIW[58,61], UCDW[58], LCDW[59] and AABW[60]). At the mid-15-kyr event, UCDW, LCDW, AABW, the corals at our site and the Icelandic records all converge to ~50‰. It has been suggested that Arctic overflow waters are influencing the $\Delta^{14}C$ signature at our site. Although that is possible, the Arctic is unlikely to be able to affect the $\Delta^{14}C$ of our site as well as UCDW, LCDW and AABW. Therefore, we believe it is much more likely that some vertical

convection is causing Southern Ocean waters all to have similar $\Delta^{14}C$ values, and some southern-sourced waters are influencing the $\Delta^{14}C$ of our site as well as perhaps waters near Iceland (as previously suggested[63]).

Evidence and mechanism for southern sourced waters to our site. Owing to inefficient carbon isotope exchange in the outcrop regions, southern-sourced waters tend to be $\Delta^{14}C$ depleted. Both the $\Delta^{14}C$ and heating at the deep-water formation zones in the Southern Hemisphere could be transferred to near our site by the deep circulation. Then a pre-Bølling–Allerød shift in deep-water structure (potentially caused by winds or buoyancy fluxes in the Southern Ocean, or both) could have caused this warm front to cross our site from deeper waters to shallower. Indeed, Antarctic ice cores and Southern Ocean sea surface temperature records show a sustained temperature rise from ~17.8 kyr ago to the start of the Bølling–Allerød[1,64].

Further evidence of southern-sourced water is seen in previous Cd/Ca measurements[10] made on two of the corals in our study, which show the pre-Bølling–Allerød warmth and $\Delta^{14}C$-depletion signature. These data show that the warmth and $\Delta^{14}C$-depletion signature is associated with an increase in Cd/Ca by a factor of two, which is consistent with an influx of high-nutrient or Southern-sourced waters coming to our site. This increase in Cd/Ca during HS1 has also previously been seen in benthic foraminifera from a core off Iceland[63].

Northward penetration of southern-sourced intermediate waters during deglaciation has been controversial. Several studies report increased northward penetration during the Younger Dryas and HS1[10,63,65], while others suggest that there was a weakening of penetration of AAIW during the deglaciation[66,67]. Sites that have reported increased northward penetration are in general deeper than the modern expression of AAIW, while shallower sites (<1,000 m) do not see AAIW during the deglaciation. Our data suggest increased northward penetration of southern-sourced waters at much greater depths than seen today, consistent with previous studies and several modelling studies[6,68].

Comparison with other Atlantic $\delta^{13}C$ records. High-resolution records from the Atlantic were compiled for the past 20 kyr (refs 39–43, 53; Extended Data Fig. 8). Similar to previous compilations[39], sections of $\delta^{13}C$ show a vertically stratified ocean at the LGM with very large $\delta^{13}C$ differences between southern and northern end-members compared with the modern $\delta^{13}C$ of DIC[39]. Our new compilations of four other time slices during the last deglaciation provide a view into when the ocean reorganized from an LGM to a modern-like circulation state. In the early part of the deglaciation the upper waters changed more than the deepest waters, reflecting a more dynamic interplay between northern- and southern-sourced intermediate and upper deep waters. These data are consistent with a deep stratification at ~2,000 m water depth at the LGM and during the early deglaciation[69,70]. This comparable lack of circulation dynamics in the abyssal Atlantic altered drastically at the HS1/Bølling–Allerød transition, when the very deep southern-sourced[20] water mass became much less depleted and volumetrically less important. Thus, we characterize the Bølling–Allerød as the moment when a modern-like configuration first appears. The Younger Dryas has previously been thought to reflect a return to Heinrich-like conditions; however, the $\delta^{13}C$ sections indicate that, rather than being similar to HS1, over time during the Younger Dryas the deep two-cell circulation structure changed to a more modern interleaving of northern and southern water masses.

31. Thiagarajan, N. *et al.* Movement of deep-sea coral populations on climatic timescales. *Paleoceanography* **28,** 227–236 (2013).
32. Robinson, L. F. *et al.* Deep-sea scleractinian coral age and depth distributions in the northwest Atlantic for the last 225,000 years. *Bull. Mar. Sci.* **81,** 371–391 (2007).
33. Cheng, H., Adkins, J. F., Edwards, R. L. & Boyle, E. A. U-Th dating of deep-sea corals. *Geochim. Cosmochim. Acta* **64,** 2401–2416 (2000).
34. Reimer, P. J. *et al.* IntCal09 and Marine09 radiocarbon age calibration curves, 0-50,000 years cal BP. *Radiocarbon* **51,** 1111–1150 (2009).
35. Passey, B. H., Levin, N. E., Cerling, T. E., Brown, F. H. & Eiler, J. M. High-temperature environments of human evolution in East Africa based on bond ordering in paleosol carbonates. *Proc. Natl Acad. Sci.* **107,** 11245–11249 (2010).
36. Huntington, K. W. *et al.* Methods and limitations of 'clumped' CO2 isotope (Δ_{47}) analysis by gas-source isotope ratio mass spectrometry. *J. Mass Spectrom.* **44,** 1318–1329 (2009).
37. Ghosh, P. *et al.* ^{13}C-^{18}O bonds in carbonate minerals: a new kind of paleothermometer. *Geochim. Cosmochim. Acta* **70,** 1439–1456 (2006).
38. Thiagarajan, N., Guo, W. F., Adkins, J. & Eiler, J. Clumped isotope calibration of modern deep sea corals and implications for vital effects. *Geochim. Cosmochim. Acta* **75** 4416–4425 (2009).
39. Curry, W. B. & Oppo, D. Glacial water mass geometry and the distribution of $\delta^{13}C$ of total CO_2 in the Western Atlantic Ocean. *Paleoceanography* **20,** PA1017 (2005).
40. Waelbroeck, C. *et al.* The timing of deglacial circulation changes in the Atlantic. *Paleoceanography* **26,** PA3213 (2011).
41. Oppo, D. W. & Curry, W. B. Deep Atlantic circulation during the Last Glacial Maximum and deglaciation. *Nature Edu. Knowl.* **3,** 1 (2012).
42. Marchal, O. & Curry, W. B. On the abyssal circulation in the glacial Atlantic. *J. Phys. Oceanogr.* **38,** 2014–2037 (2008).
43. Tessin, A. C. & Lund, D. C. Isotopically depleted carbon in the mid-depth South Atlantic during the last deglaciation. *Paleoceanography* **28,** 296–306 (2013).
44. Kiefer, T. & Kienast, M. Patterns of deglacial warming in the Pacific Ocean: a review with emphasis on the time interval of Heinrich event 1. *Quat. Sci. Rev.* **24,** 1063–1081 (2005).
45. Dwyer, G. S., Cronin, T. M., Baker, P. A. & Rodriguez-Lazaro, J. Changes in North Atlantic deep-sea temperature during climatic fluctuations of the last 25,000 years based on ostracode Mg/Ca ratios. *Geochem. Geophys. Geosyst.* **1,** 1028 (2000).
46. Chiessi, C. M. *et al.* South Atlantic interocean exchange as the trigger for the Bølling warm event. *Geology* **36,** 919–922 (2008).
47. Wang, Y. J. *et al.* A high-resolution absolute-dated late Pleistocene monsoon record from Hulu Cave, China. *Science* **294,** 2345–2348 (2001).
48. Adkins, J. F. & Boyle, E. A. Changing atmospheric Delta C-14 and the record of deep water paleoventilation ages. *Paleoceanography* **12,** 337–344 (1997).
49. Came, R. *et al.* Coupling of surface temperatures and atmospheric CO_2 concentrations during the Palaeozoic era. *Nature* **449,** 198–201 (2007).
50. Tripati, A., Thiagarajan, N. & Eiler, J. 'Clumped isotope' thermometry in foraminifera. *Geochim. Cosmochim. Acta* **72,** A956 (2008).
51. Emile-Geay, J. & Madec, G. Geothermal heating, diapycnal mixing and the abyssal circulation. *Ocean Sci.* **5,** 203–217 (2009).
52. Rühlemann, C., Mulitza, S., Muller, P. J., Wefer, G. & Zahn, R. Warming of the tropical Atlantic Ocean and slowdown of thermohaline circulation during the last deglaciation. *Nature* **402,** 511–514 (1999).
53. Thornalley, D. J. R., Elderfield, H. & McCave, I. N. Intermediate and deep water paleoceanography of the northern North Atlantic over the past 21,000 years. *Paleoceanography* **25,** PA1211 (2010).
54. Siani, G. *et al.* Mediterranean Sea surface radiocarbon reservoir age changes since the last glacial maximum. *Science* **294,** 1917–1920 (2001).
55. McCulloch, M. *et al.* Proliferation and demise of deep-sea corals in the Mediterranean during the Younger Dryas. *Earth Planet. Sci. Lett.* **298,** 143–152 (2010).
56. Skinner, L. & Elderfield, H. Rapid fluctuations in the deep North Atlantic heat budget during the last glacial period. *Paleoceanography* **22,** PA1205 (2007).
57. Skinner, L. & Shackleton, N. J. Rapid transient changes in northeast Atlantic deep water ventilation age across Termination 1. *Paleoceanography* **19,** PA2005 (2004).
58. Burke, A. & Robinson, L. F. The Southern Ocean's role in carbon exchange during the Last Deglaciation. *Science* **335,** 557–561 (2012).
59. Skinner, L. C., Fallon, S., Waelbroeck, C., Michel, E. & Barker, S. Ventilation of the deep Southern Ocean and deglacial CO_2 rise. *Science* **328,** 1147–1151 (2010).
60. Barker, S., Knorr, G., Vautravers, M. J., Diz, P. & Skinner, L. C. Extreme deepening of the Atlantic overturning circulation during deglaciation. *Nature Geosci.* **3,** 567–571 (2010).
61. De Pol-Holz, R., Keigwin, L., Southon, J., Hebbeln, D. & Mohtadi, M. No signature of abyssal carbon in intermediate waters off Chile during deglaciation. *Nature Geosci* **3,** 192–195 (2010).
62. Cléroux, C., deMenocal, P. & Guilderson, T. Deglacial radiocarbon history of tropical Atlantic thermocline waters: absence of CO_2 reservoir purging signal. *Quat. Sci. Rev.* **30,** 1875–1882 (2011).
63. Rickaby, R. E. M. & Elderfield, H. Evidence from the high-latitude North Atlantic for variations in Antarctic Intermediate water flow during the last deglaciation. *Geochem. Geophys. Geosyst.* **6,** Q05001 (2005).
64. Sachs, J. P., Anderson, R. F. & Lehman, S. J. Glacial surface temperatures of the Southeast Atlantic Ocean. *Science* **293,** 2077–2079 (2001).
65. Pahnke, K., Goldstein, S. & Hemming, S. Abrupt changes in Antarctic Intermediate Water circulation over the past 25,000 years. *Nature Geosci.* **1,** 870–874 (2008).
66. Xie, R. C., Marcantonio, F. & Schmidt, M. W. Deglacial variability of Antarctic Intermediate Water penetration into the North Atlantic from authigenic neodymium isotope ratios. *Paleoceanography* **27,** PA3221 (2012).
67. Came, R. E., Oppo, D. W., Curry, W. B. & Lynch-Stieglitz, J. Deglacial variability in the surface return flow of the Atlantic meridional overturning circulation. *Paleoceanography* **23,** PA1217 (2008).
68. Saenko, O. A., Weaver, A. J. & Gregory, J. M. On the link between the two modes of the ocean thermohaline circulation and the formation of global-scale water masses. *J. Clim.* **16,** 2797–2801 (2003).
69. Lund, D. C., Adkins, J. F. & Ferrari, R. Abyssal Atlantic circulation during the Last Glacial Maximum: constraining the ratio between transport and vertical mixing. *Paleoceanography* **26,** PA1213 (2011).
70. Adkins, J. F. The role of deep ocean circulation in setting glacial climates. *Paleoceanography* **28,** 539–561 (2013).
71. Eltgroth, S. F., Adkins, J. F., Robinson, L., Southon, J. & Kashgarian, M. A deep-sea coral record of North Atlantic radiocarbon through the Younger Dryas: Evidence for Intermediate/Deep water reorganization. *Paleoceanography* **21,** PA4207 (2006).
72. Keigwin, L. D. Radiocarbon and stable isotope constraints on Last Glacial Maximum and Younger Dryas ventilation in the western North Atlantic. *Paleoceanography* **19,** PA4012 (2004).

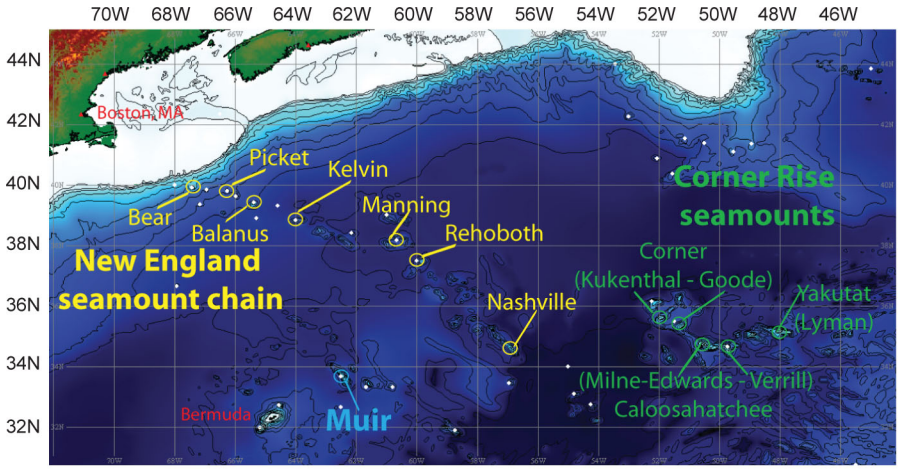

Extended Data Figure 1 | Sample collection sites. Sites of sample collection in the North Atlantic.

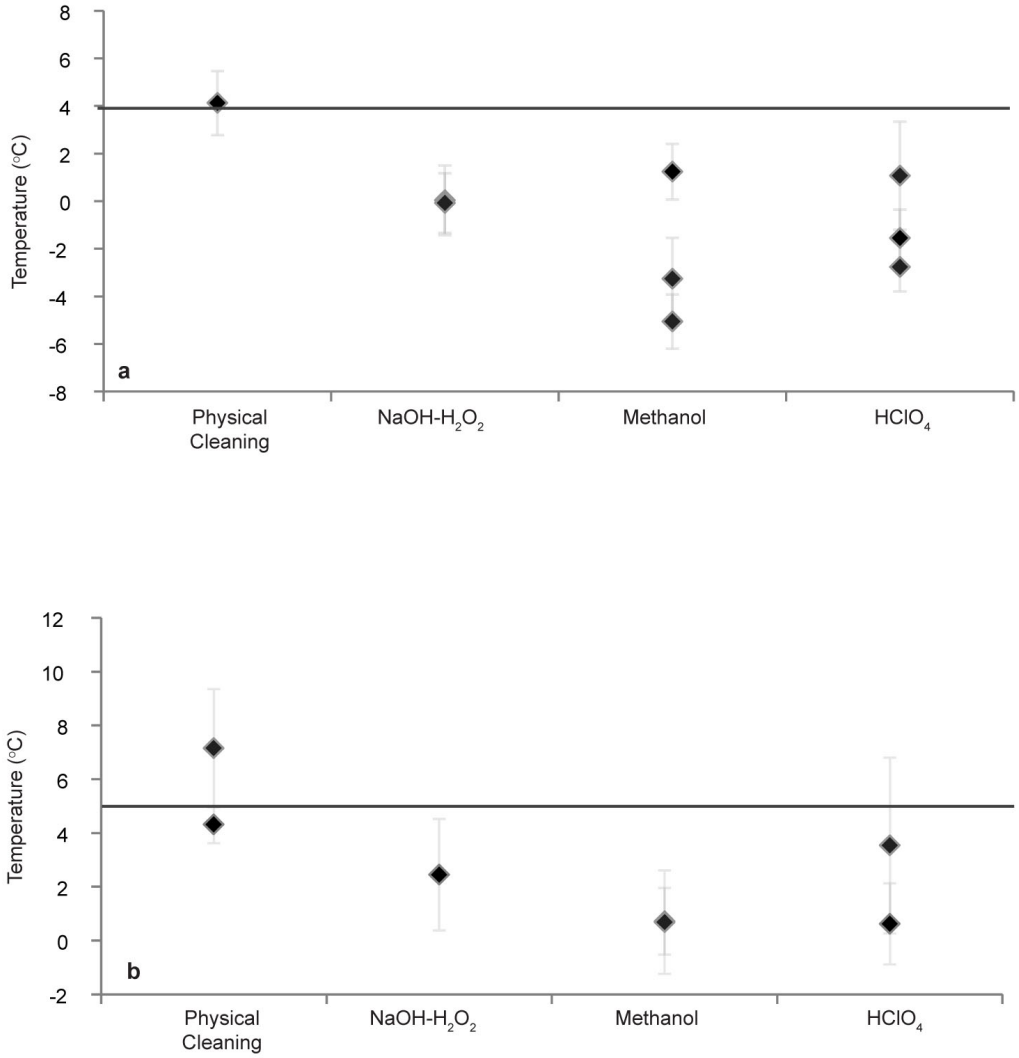

Extended Data Figure 2 | Δ_{47} cleaning study. Two different modern corals were selected to determine which cleaning method did not bias Δ_{47} temperatures. A live-when-collected coral with a growth temperature of 3.9 °C (**a**) and a coral with an Fe–Mn crust and a ^{14}C age matching that of the modern water column from 5 °C waters in the Southern Ocean (**b**) were selected for the cleaning study. We found that physical cleaning with a Dremel tool gave accurate Δ_{47}–temperature reconstructions. Error bars are 1 s.e.m.

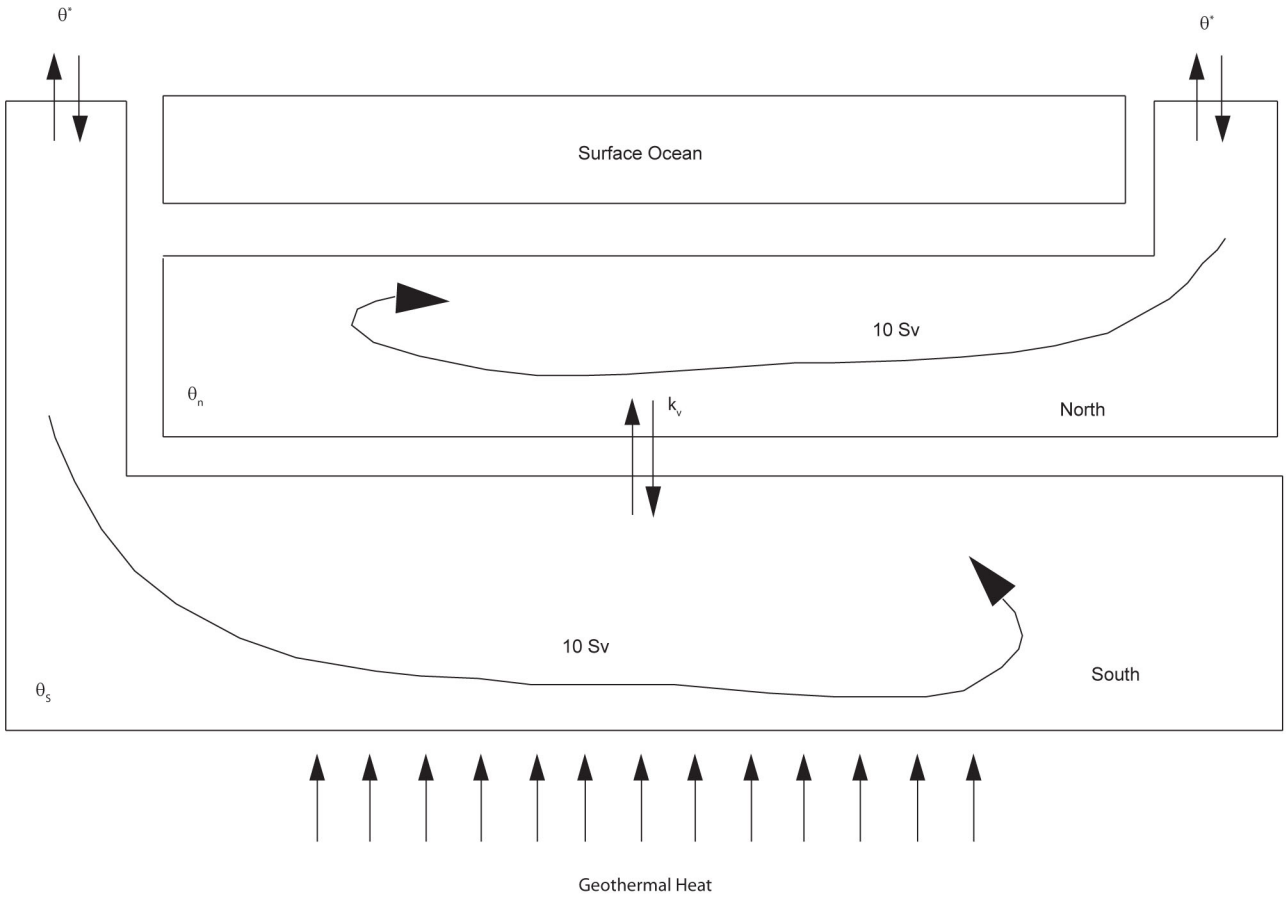

$$C_p V_s \frac{d\Theta}{dt} = F_{gh} A - p q_s C_p (\Theta_s - \Theta_s^*) - k_v C_p \rho \frac{V_s}{A} V_s (\Theta_s - \Theta_n)$$

$$C_p V_n \frac{d\Theta}{dt} = -p q_n C_p (\Theta_n - \Theta_n^*) + k_v C_p \rho \frac{V_s}{A} V_s (\Theta_s - \Theta_n)$$

Extended Data Figure 3 | Box model and equations. This schematic describes the box model and equations used to calculate the effect of geothermal heat on ocean temperatures. C_p is the heat capacity of sea water, V is the volume fraction of the northern or southern box, Θ is the temperature, ρ is the density of sea water, q is the overturning rate of the northern or southern box, A is the area of the ocean, k_v is the vertical mixing coefficient and F_{gh} is the geothermal heat flux (0.1 W m^{-2}).

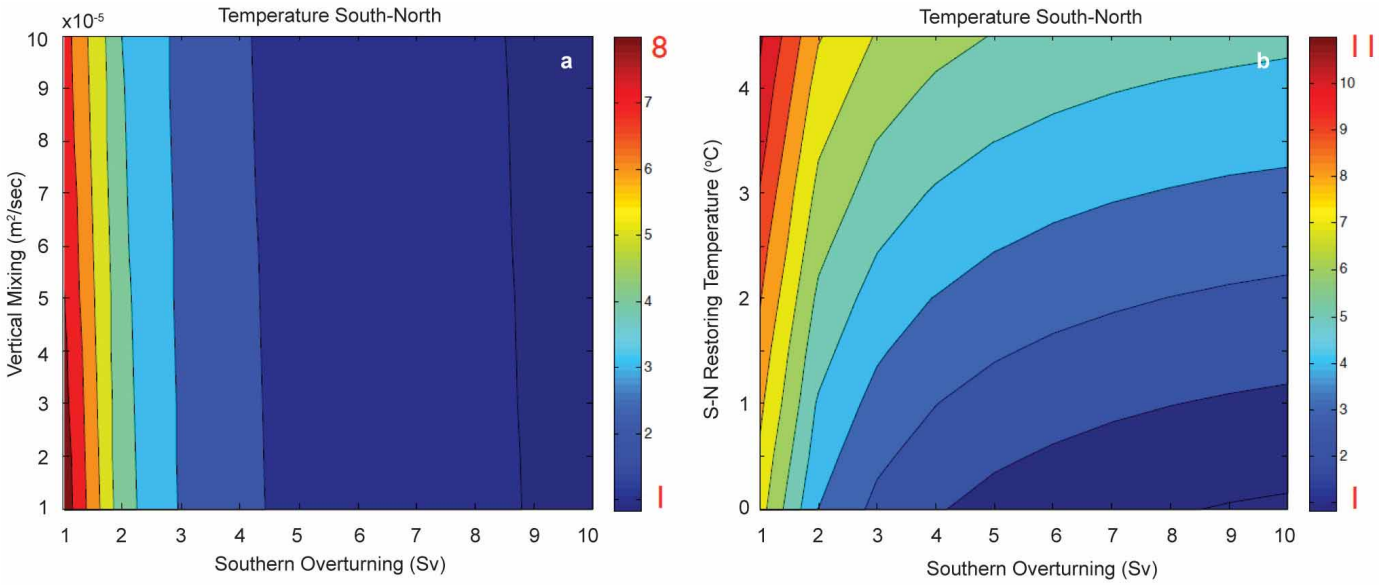

Extended Data Figure 4 | Steady-state temperature change with ocean overturning and mixing. The steady-state solutions for the box model in Extended Data 3. **a**, If there is a well-flushed southern cell (10 Sv of overturning), the bottom water is only warmed by about 0.8 °C relative to the restoring temperature in the atmosphere. However, for a very slow overturning (1 Sv) this temperature increase can reach over 8 °C, well above the temperature change seen at our site. **b**, Increasing the difference between the restoring temperature in the south relative to the north can increase the warming by as much as 11 °C (Supplementary Fig. 4b).

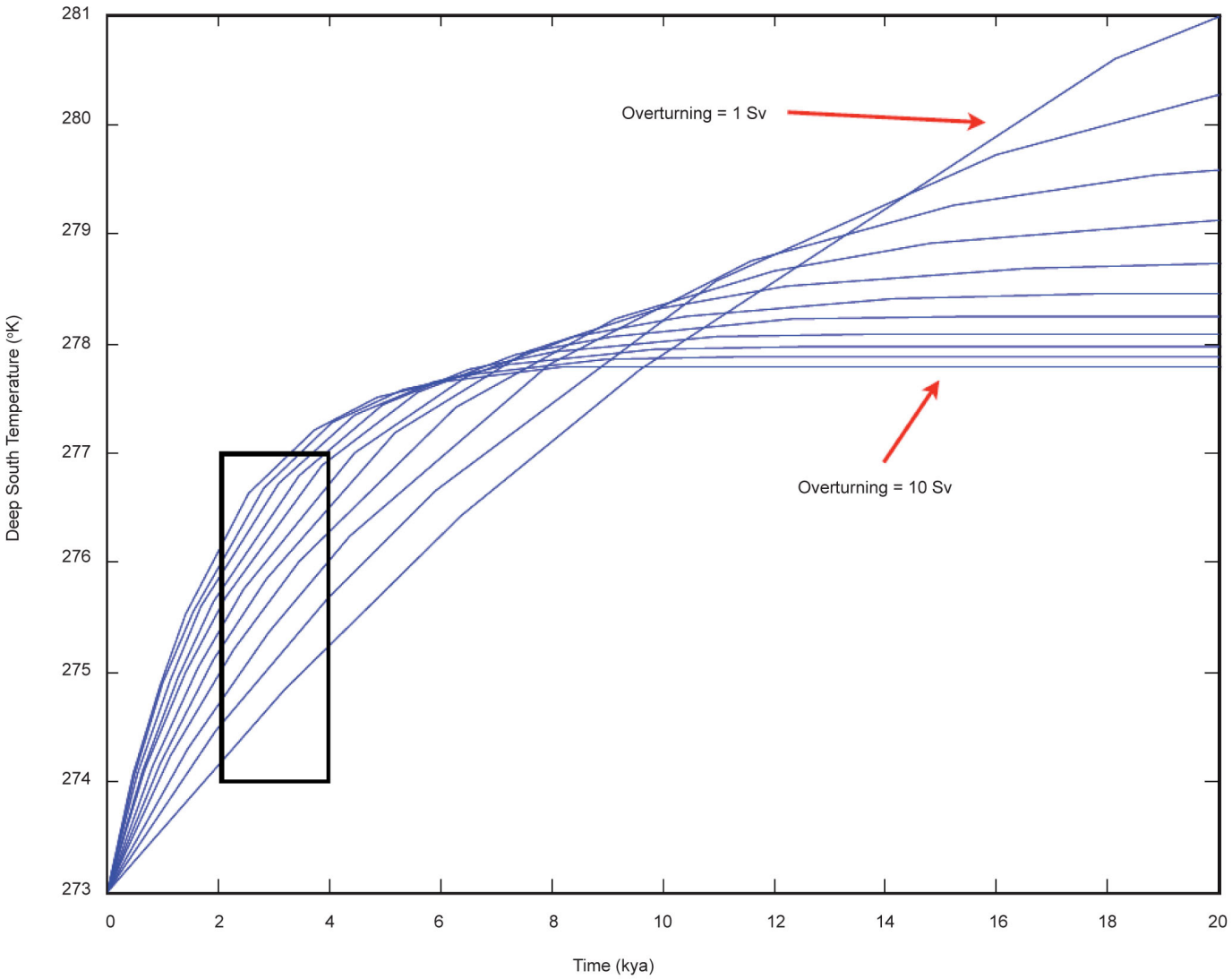

Extended Data Figure 5 | Transient-state temperature change with ocean overturning and mixing. The transient-state solution for the box model in Extended Data 3. The vertical diffusivity was kept constant and the Southern Hemisphere restoring temperature at 277 K. We find that there is a rapid warming within the first few thousand years (denoted by the black box).

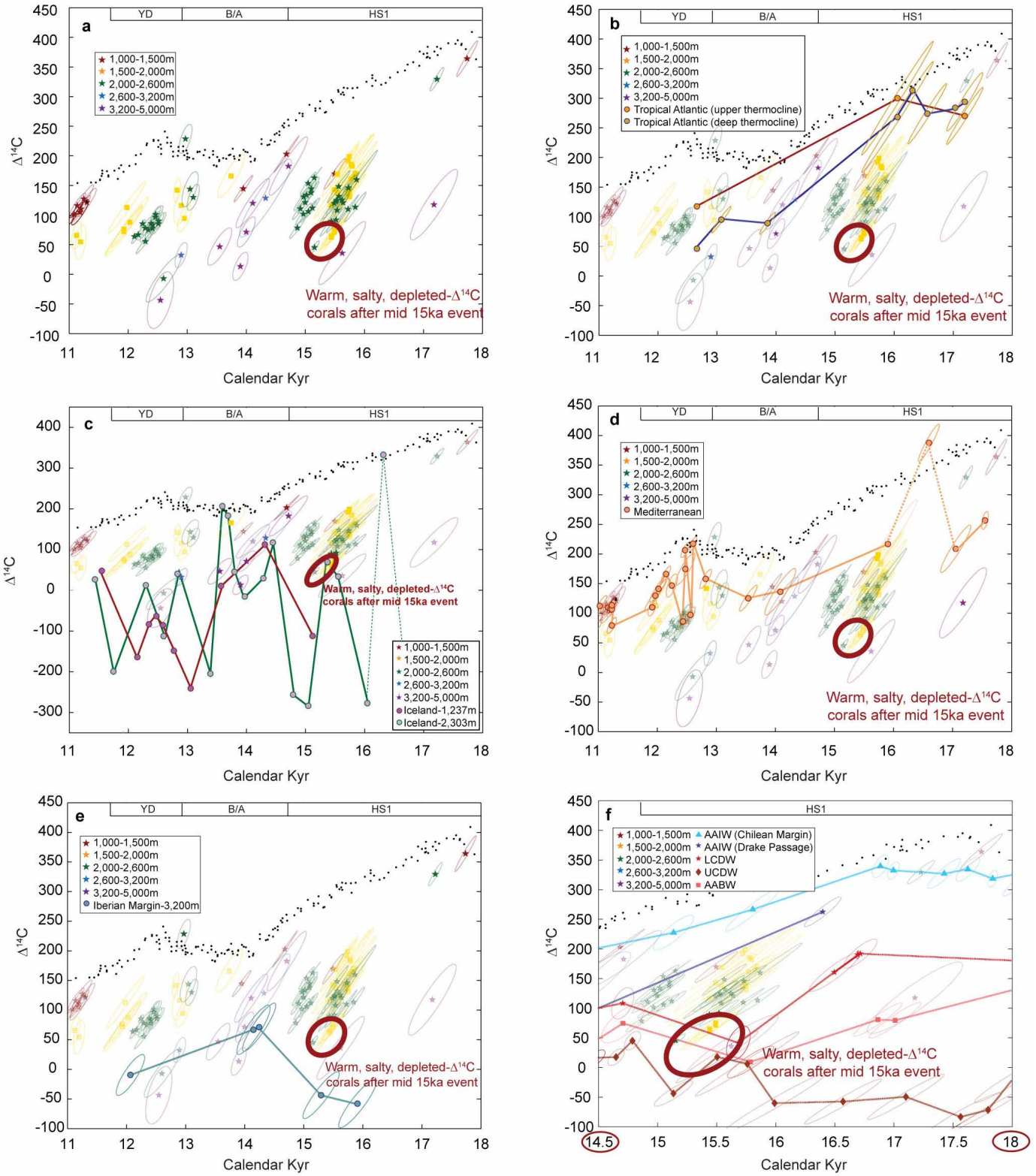

Extended Data Figure 6 | Comparison with other $\Delta^{14}C$ records during the deglaciation. A comparison of the $\Delta^{14}C$ of deep-sea corals (previously published work[11,71] and current study) and foraminifera[72] from the Northwest Atlantic (**a**) with $\Delta^{14}C$ of the tropical Atlantic[62] (**b**), Iceland[53] (**c**), the Mediterranean[54,55] (**d**), the Iberian margin[57] (**e**) and the Southern Ocean[58–61] (**f**). The three corals from our study showing a warm and $\Delta^{14}C$-depleted signature at 15 kyr ago are circled in red. Although the tropical Atlantic and Mediterranean are both warm, they have too-enriched $\Delta^{14}C$ values to explain the warm, $\Delta^{14}C$-depleted water seen at our site at the mid-15-kyr event. Iceland has extremely $\Delta^{14}C$-depleted waters, but these are thought to form during brine formation, which would not generate warm waters. The Iberian margin also has $\Delta^{14}C$ values, but it is bathed by cooler waters and does not show the abrupt mid-15-kyr warming (Extended Data 7). At the mid-15-kyr event, UCDW, LCDW, AABW, the corals at our site and the Icelandic records all converge to ~50‰. We believe it is much more likely that some vertical convection is causing Southern Ocean waters all to have similar $\Delta^{14}C$ values, and that some southern-sourced waters are influencing the $\Delta^{14}C$ of our site as well as perhaps waters near Iceland (as previously suggested[63]). Note the different axes on **f**. (Points in **c** and **d** that are above the atmospheric value are connected with a dashed line instead of a solid line.) Uncertainties are 2σ error ellipses except for the Iberian margin and Mediterranean records, which are 1σ.

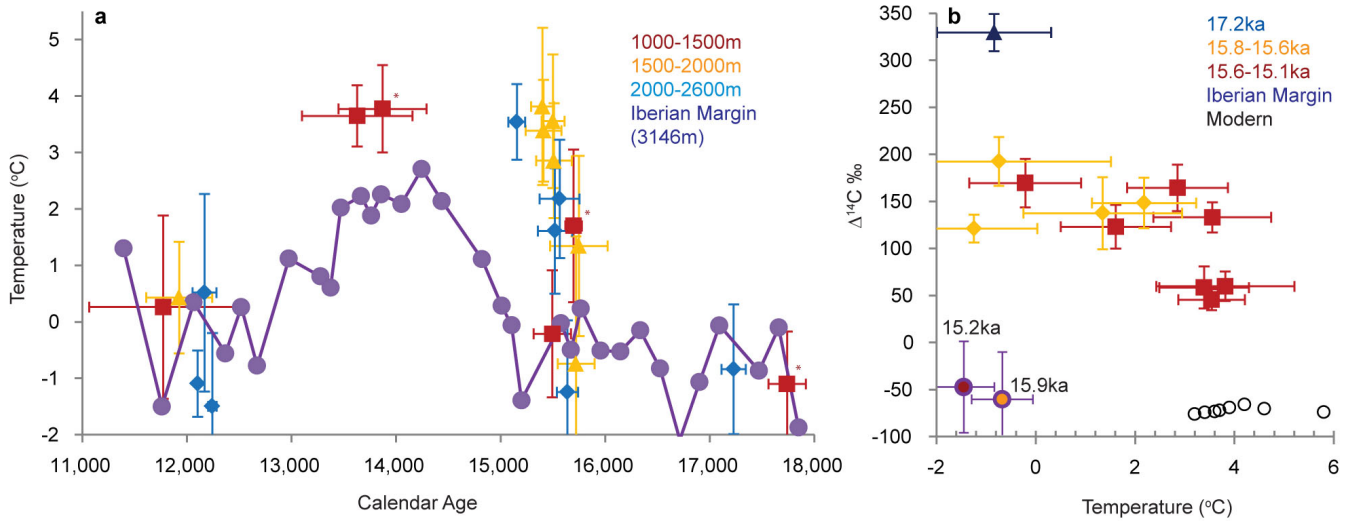

Extended Data Figure 7 | Comparison with Iberian margin $\Delta^{14}C$ and temperature. a, A comparison of the Mg/Ca–temperature and $\Delta^{14}C$ record from the Iberian margin[57] with the record from our site. The Iberian margin shows a warming at the beginning of the Bølling–Allerød but not an abrupt mid-15-kyr warming. Asterisks indicate corals which have either a high $\delta^{234}U_i$ or a $\Delta^{14}C$ above the atmospheric value. In both cases, this open-system behaviour changes the $\Delta^{14}C$ values but does not change calendar ages much on this plot. **b**, $\Delta^{14}C$ measurements at the Iberian margin also show that the water bathing the Iberian margin is distinct from the warm and $\Delta^{14}C$-depleted water at our site. Error bars are 1 s.e.m.

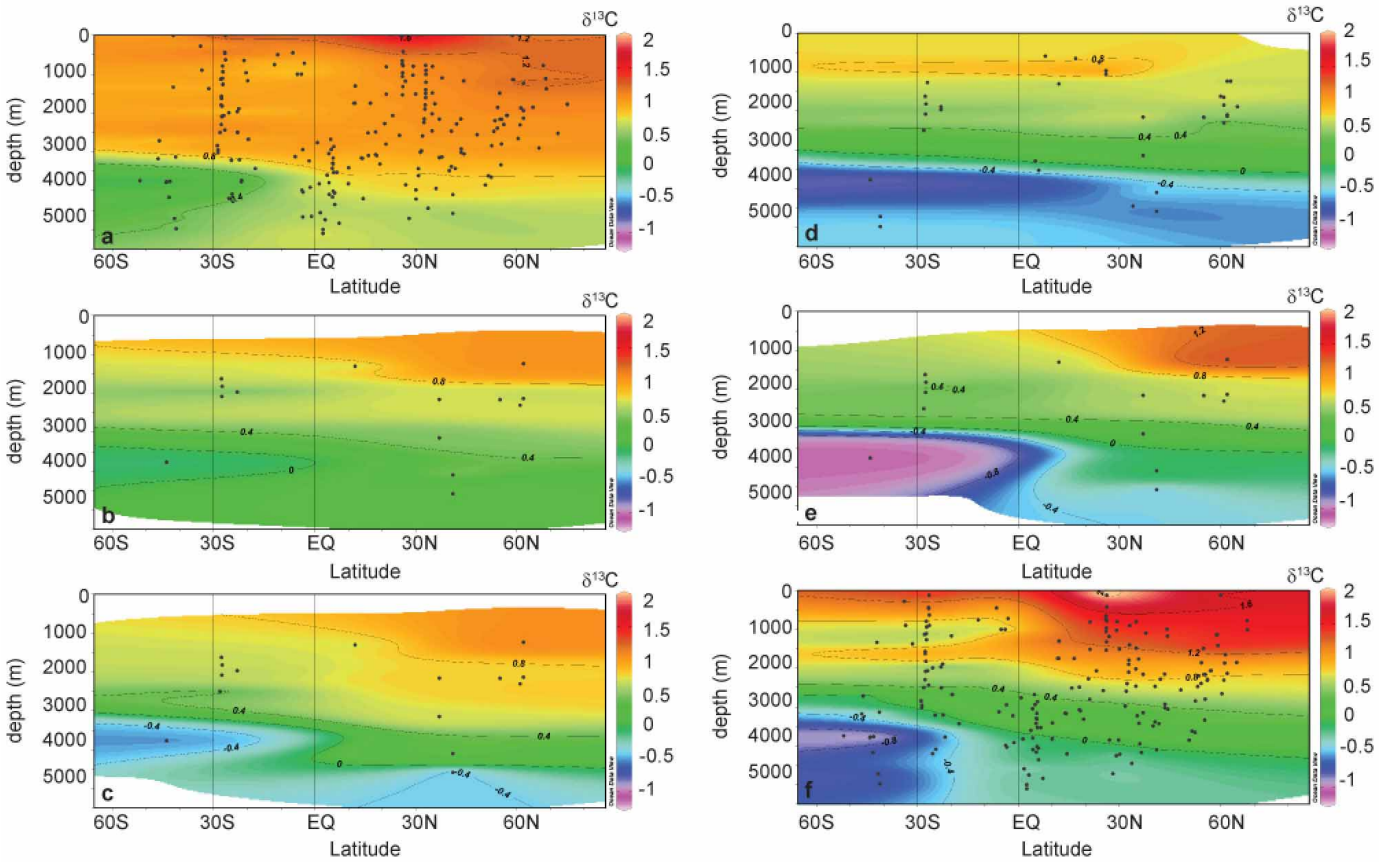

Extended Data Figure 8 | Compilation of Atlantic benthic $\delta^{13}C$ records. **a**, Benthic sections of $\delta^{13}C$ from well-dated, high-resolution cores[39–43,53] in the North Atlantic as well as from the GEOSECS database. Black dots indicate the latitudes and depths of cores used to make the sections. The time intervals compiled are as follows: Holocene (0–10 kyr ago; **a**), Younger Dryas (11.7–13 kyr ago; **b**), Bølling–Allerød (13–14.5 kyr ago; **c**), late HS1 (14.5–15.7 kyr ago; **d**), early HS1 (15.7–18 kyr ago; **e**), Last Glacial Maximum (19–22 kyr ago; **f**). At the LGM (**f**), cold, salty and $\delta^{13}C$-depleted water from the south lay below cold, fresher and $\delta^{13}C$-enriched water. During HS1 (**d**, **e**), intermediate waters changed more than deeper waters. By the Bølling–Allerød (**c**), the $\delta^{13}C$ distribution seen today had been established. The Younger Dryas (**b**), while thought to be a return to Heinrich-like water masses, is structured differently than the late-HS1 section and was a progression towards the Holocene water column configuration (**a**).